N78-24059

THEORETICAL PREDICTIONS OF JET INTERACTION EFFECTS FOR USB AND OWB CONFIGURATIONS*

C. Edward Lan
The University of Kansas

James F. Campbell
NASA Langley Research Center

13

SUMMARY

A wing-jet interaction theory is presented for predicting the aerodynamic characteristics of upper-surface-blowing and over-wing-blowing configurations. For the latter configurations, a new jet entrainment theory has also been developed. Comparison of predicted results with some available data showed good agreement. Some applications of the theory are also presented.

INTRODUCTION

When a wing is in close proximity to a jet, additional forces and moments will be induced on the wing. In the case of upper-surface-blowing (USB) configurations, where the relatively thick jet from the high bypass-ratio turbofan engines blows on the wing upper surface, these forces and moments can not be satisfactorily explained by the thin jet flap theory (ref. 1). With an over-wing-blowing (OWB) configuration, the conventional jet engine exhaust may be blowing aft or ahead of the wing leading edge and close to or away from the wing surface. It has been found that its wing aerodynamic characteristics are underpredicted by entrainment effects alone, in particular, when the jet is close to the wing surface (ref. 2). It is evident, then, that additional physical mechanisms for these effects must be identified. In this paper, they will be called the "jet interaction effects." By "interaction," it is implied that in the physical process, not only the wing flow field is perturbed in the presence of the jet, but also the jet flow is disturbed by the wing as well.

In the past, this jet interaction process has been applied mainly in the wing-slipstream interaction problem. For example, Shollenberger (ref. 3) developed a method wherein the jet shape distortion is allowed in predicting interaction effects. However, it is not applicable to the case where the jet Mach number is different from the freestream value (Mach number nonuniformity) and its applications to USB or OWB configurations have not been reported. On the other hand, Mendenhall et al. (ref. 4) used several circular jets with

*This work was supported by NASA Langley Research Center under grant NSG 1139 for the first author.

prescribed boundaries to approximate a rectangular USB jet without including the interaction process mentioned above.

In developing the analytical method for OWB configurations, Krenz (ref. 5) used sink panels on prescribed jet boundaries. No systematic method of computing the sink strength at arbitrary jet velocity ratios has been presented. To simulate the jet entrainment effect, Putnam (ref. 6) obtained the sink strength of a line sink distribution along the jet axis by Squire and Trouncer's method for incompressible, non-heated jets (ref. 7). In both studies, no interaction effects have been accounted for.

In this paper, results from a theoretical investigation of jet interaction effects for USB and OWB configurations in the past two years will be summarized. The present theory accounts for differences between the jet and free-stream dynamic pressures and Mach numbers. The jet shape can be rectangular or circular and the jet exit can be at an arbitrary location. However, the theory is a linear one so that the jet boundary distortion is not accounted for.

SYMBOLS

Values are given in both SI and U.S. Customary Units. The measurements and calculations were made in U.S. Customary Units.

AR	wing aspect ratio
c	chord length, m (ft)
$C_{D,i}$	induced drag coefficient
C_L	total lift coefficient
ΔC_L	difference in lift coefficients with jet on and off
C_m	pitching-moment coefficient
C_μ	jet-momentum coefficient
C'_μ	jet-momentum coefficient referred to p_∞
D_o	jet exit diameter, m (ft)
$\vec{e}$	unit vector tangent to jet path
$\vec{k}$	a unit vector along the z-axis

M_j	jet Mach number
M_∞	freestream Mach number
$\hat{n}$	unit vector normal to jet surface
r,s	jet axis system, normal and tangent to the jet surface, respectively
p_∞	ambient static pressure, N/m^2 (lb/ft^2)
$p_{t,n}$	nozzle total pressure, N/m^2 (lb/ft^2)
s	$= V_j/V_o$
S	wing area, m^2(ft^2)
T	$= \rho_\infty/\rho_j$
V_j	jet velocity, m/sec (ft/sec)
V_o	outer flow velocity, m/sec (ft/sec)
$\vec{V}_{je}$	jet-entrained flow vector, m/sec (ft/sec)
$\vec{V}_\infty$	freestream velocity vector, m/sec (ft/sec)
x,y,z	wing-fixed rectangular coordinates with positive x-axis along axis of symmetry pointing downstream, positive y-axis pointing to right, and positive z-axis pointing upward, m (ft)
x_j	jet exit coordinate, m (ft)
z_c	camber function, $z_c = z_c(x,y)$
z_j	height of jet axis above the wing plane, m (ft)
α	angle of attack, deg
Γ	vortex strength, m^2/sec (ft^2/sec)
δ_f	flap angle, deg
δ_j	jet-deflection, deg

λ	taper ratio
Λ_L	leading-edge sweep angle, deg
μ	$= V_\infty/V_j$
μ'	$= \vec{V}_\infty.\vec{e}/\vec{V}_j.\vec{e}$
ρ	density, kg/m^3 ($slugs/ft^3$)
$\bar{\phi}_j$	nondimensional velocity potential for the jet flow
$\bar{\phi}_o$	nondimensional velocity potential for the outer flow

DESCRIPTION OF THE METHOD

Basic Concept

Consider a two-dimensional inviscid, incompressible flow in which a jet is situated as shown in fig. 1, where a vortex Γ is assumed to exist in the outer flow. In order to satisfy the jet surface boundary conditions which require that the streamlines at both sides of the jet surface be parallel and the static pressures there be continuous, it is necessary to introduce additional vortices as has been shown by the image method (ref. 8). For the planar jet, the lower region in which the vortex Γ originates will receive additional disturbances represented by the vortex "A" (i.e., reflection effect). If the vortex Γ is now replaced by an airfoil, these additional disturbances on the airfoil will be in the form of upwash, thus increasing the lift. The vortex "B" represents the disturbance of the jet flow by the wing. Similar explanation can be given for a circular jet. It is seen, then, that the lift increment due to jet interaction is mainly due to the reflection of wing-created disturbances at the jet surface.

Three-Dimensional Formulation

In the three-dimensional case, the image method can not be used. However, the basic concept explained above remains applicable. That is, the additional upwash on the wing due to the jet surface reflection can be computed by satisfying the jet surface boundary conditions together with the wing tangency condition. In the linear theory, these conditions can be written as (ref. 2),

$$\frac{\partial \bar{\phi}_o}{\partial n} - \frac{\partial \bar{\phi}_j}{\partial n} = -\frac{\vec{V}_\infty.\vec{n}(1-\mu')}{\vec{V}_\infty.\vec{e}} \qquad \text{jet surface tangency condition} \qquad (1)$$

$$\frac{\partial \bar{\phi}_j}{\partial s} - T(\mu')^2 \frac{\partial \bar{\phi}_o}{\partial s} = 0 \qquad \text{jet surface pressure continuity} \qquad (2)$$

$$\frac{\partial \bar{\phi}_o}{\partial z} = \frac{\partial z_c}{\partial x} - \frac{\vec{V}_o \cdot \vec{k}}{\vec{V}_\infty \cdot \vec{e}} \qquad \text{wing tangency} \qquad (3)$$

where

$$\vec{V}_o = \vec{V}_\infty + \vec{v}_{je} \qquad (4)$$

and $\vec{v}_{je}$ is the jet-entrained flow vector. To satisfy eqs. (1)-(2), the jet surface is replaced by two vortex sheets -- one to account for the perturbations in the outer flow and the other for the jet flow. This is necessary because of the Mach number nonuniformity. Eq. (3) is satisfied in the usual manner with a wing vortex sheet. The results are then reduced to algebraic equations for unknown vortex strengths through the application of a quasi-vortex-lattice method (ref. 1). This vortex model is illustrated in fig. 2. Note that for USB configurations, the jet entrainment is not directly included. Instead, it enters the problem through the Coanda jet reaction, because the Coanda turning is due to the jet entrainment. The Coanda jet reaction is calculated here with the linear momentum principle and is illustrated in fig. 3. It is seen that the total lift component due to the Coanda jet reaction is

$$\begin{aligned} C_{L,R} &= 2C_\mu \sin(\delta_j/2) \cos(\delta_j/2 + \alpha) + C_\mu \sin\alpha \\ &= C_\mu \sin(\delta_j + \alpha) \end{aligned} \qquad (5)$$

Similarly, drag component due to the Coanda jet reaction is given by

$$\begin{aligned} C_{D,R} &= 2C_\mu \sin(\delta_j/2) \sin(\delta_j/2 + \alpha) - (C_\mu \cos\alpha - \mu C_\mu) \\ &= C_\mu [\mu - \cos(\delta_j + \alpha)] \end{aligned} \qquad (6)$$

where the thrust component is also included. The jet flap effect is also calculated in the present method as described in ref. 1.

On the other hand, for OWB applications, the jet entrainment is calculated according to a newly developed method (ref. 2) which is applicable to a compressible heated jet. To avoid nonhomogeneous jet propertics in the mathematical model, an equivalent uniform jet is used which satisfies the conserva-

tion of mass, linear momentum and heat content. If the jet does not intersect the wing, a circular jet is assumed. This circular jet is in turn approximated by a polygon for interaction computation. In case the jet intersects the wing, a rectangular or circular jet may be chosen in the calculation, depending on whether or not the jet would follow the wing surface and deflect at the trailing edge at some angle relative to the chord line. This deflection angle can only be determined empirically at present by correlation with experimental data.

COMPARISON WITH EXPERIMENTAL DATA

In comparing the USB data, the calculations were done with experimental jet deflection angles measured under wind-off conditions. The data of a transport-type configuration of Smith, et al. (ref. 9) with AR = 7.8, λ = 0.73 and Λ_L = 0° are compared in fig. 4. The moment arms for the Coanda forces are measured directly from fig. 3 of ref. 9. The skin friction and the scrubbing drags are not accounted for in the moment computation. It is seen that the predicted results agree reasonably well with the data. It should be noted that all results were obtained by adding the predicted jet-induced increments to the experimental jet-off values. Since the method also predicts the induced drag, its comparison can be made approximately by using the relation:

$$\Delta C_{D,(\alpha)} = (C_{D,i} + C_{D,R})_{(\alpha)} - (C_{D,i} + C_{D,R})_{(\alpha = 1°)} \qquad (7)$$

Eq. (7) approximately represents the incremental induced drag due to the angle of attack. The results are compared in the following table with good agreement:

δ_f	0°		20°		40°		60°	
	$\Delta C_{D,(\alpha)}$		$\Delta C_{D,(\alpha)}$		$\Delta C_{D,(\alpha)}$		$\Delta C_{D,(\alpha)}$	
α	Theory	Exp.	Theory	Exp.	Theory	Exp.	Theory	Exp.
6°	0.096	0.15	0.233	0.2	0.322	0.3	0.375	0.35
11°	0.227	0.3	0.5	0.5	0.658	0.6	0.752	0.65

The jet induced lift increments for a fighter, vectored-thrust (VT) configuration of AR = 3.7 given in ref. 10 are compared in fig. 5. Since the model airfoil is thin (5%) and the camber is of supercritical type but unknown, it was assumed to be a flat wing in the computation to simulate the

jet-off C_L as closely as possible. As the jet Mach number is mostly supersonic, which is not allowed in the present subsonic computer program, the jet Mach number is assumed to be M_∞ and an equivalent velocity ratio is used as described in ref. 6. If the static thrust coefficient is C'_μ nondimensionalized with the ambient pressure, then C_μ in terms of freestream dynamic pressure is given by

$$C_\mu = \frac{2C'_\mu}{\gamma M_\infty^2} \qquad 8)$$

where C'_μ is given in ref. 10 and γ is the ratio of specific heats. From the comparison, it is seen that the agreement is reasonably good.

The OWB data by Falk (ref. 11) and Putnam (ref. 12) are compared with the predicted results in figs. 6 and 7, respectively. From fig. 6, it is seen that ΔC_L decreases rapidly as the jet is moved upwards from the wing surface. This is because with the jet close to the wing, the interaction effects become important. In addition, if the jet intersects the wing, the jet flap effect due to the jet deflection at the trailing edge relative to the chord line will also be significant. Both effects diminish rapidly with the distance to the wing surface. It is also seen from both figs. 6 and 7 that jet entrainment alone will underpredict ΔC_L if the jet is close to the wing.

SOME ADDITIONAL RESULTS

As mentioned above, the jet interaction effects are mainly due to the jet surface reflection of wing-created disturbances which are proportional to the jet-off wing loading. Therefore, it is important in the interaction computation to simulate the jet-off lift as closely as possible. To see how the jet-off lift can affect the interaction effects, the configuration of Smith, et al. given in ref. 9, is again used under the conditions of $\alpha = 1°$, $\delta_f = 0°$, $\delta_j = 12°$ and $C_\mu = 2$. If NACA 64_2A215 (a = 0.5) and NACA 64_1A412 (a = 0.5) airfoils are used at the root and the tip, respectively, as shown in ref. 9, the theoretical jet-induced ΔC_L would be 0.826. On the other hand, if a symmetrical airfoil is used, ΔC_L becomes 0.688, a decrease of 19%. In addition, it has been shown that the jet flap effect (i.e., the effect of jet deflection relative to the chord) is always beneficial (ref. 1). That means that a thick airfoil with some trailing-edge angle will give better aerodynamic characteristics than a thin airfoil with little trailing-edge angle.

It has been shown experimentally and theoretically that the wing loading with USB has high peak in the jet region. Therefore, it is of interest to see how trade-offs can be made between lift capability and aspect ratio in cruise. Assume that $\alpha = 2°$ and $\delta_j = 10°$ without flap deflection and the jet is blowing from the leading edge. The results are shown in fig. 8. It is seen that although the lift will be decreased by 60% at $C_\mu = C$ when AR is reduced from 8 to 4, the decrease is only 42.7% in the circulation lift and 34.2% in the total lift (including the jet reaction) at $C_\mu = 1$. The decrease in the lift capability when the aspect ratio is reduced is seen to decrease as C_μ is increased.

One advantage of OWB configurations with the jet not intersecting the wing is that the jet scrubbing drag can be eliminated. Furthermore, the jet-entrainment created upwash will increase the loading and the leading-edge thrust. It is of interest to compare the interaction effects of rectangular jets with circular ones assuming the same cross-sectional area and entrainment. The jet axis is taken to be at $z_j/D_o = 1.2$ and the entrainment is computed assuming a circular jet. The results are shown in fig. 9. It is seen that both rectangular and circular jets perform equally well. However, it may be feasible to lower the rectangular jet to increase the performance without scrubbing the wing. It is also seen from the figure that the aerodynamic performance can be greatly improved by an over-wing-blowing jet, as has also been noted by Putnam (ref. 6).

CONCLUDING REMARKS

A theoretical method has been presented for predicting the aerodynamic characteristics of USB and OWB configurations. The predicted results show good agreement with some available data. The jet interaction effects have been shown to be important when the jet is on or close to the wing surface. Because of the nature of the interaction process, higher interaction lift can be achieved by increasing the jet-off lift. For a rectangular wing with USB in cruise, the total lift is shown to decrease by 34.2%, compared with 60% with jet off, when the aspect ratio is reduced from 8 to 4. It was shown for the OWB configurations that the interaction effects depend strongly on the distance of the jet surface to the wing.

REFERENCES

1. Lan, C. Edward; and Campbell, James F.: Theoretical Aerodynamics of Upper-Surface-Blowing Jet-Wing Interaction. NASA TN D-7936, 1975.

2. Lan, C. Edward: A Theoretical Investigation of Over-Wing-Blowing Aerodynamics. KU-FRL-700 (NASA Grant NSG 1139), The University of Kansas Center for Research, Inc., March 1976. (Available as NASA CR-144969.)

3. Shollenberger, C.A.: Three-Dimensional Wing/Jet Interaction Analysis Including Jet Distortion Influences. Journal of Aircraft, Vol. 11, No. 9, Sept. 1975, pp. 706-713.

4. Mendenhall, M.R.; Perkins, S.C. Jr.; Goodwin, F.K.; and Spangler, S.B.: Calculation of Static Longitudinal Aerodynamic Characteristics of STOL Aircraft with Upper-Surface-Blown Flaps. NASA CR-137646, April 1975.

5. Krenz, G.: Airframe-Engine Interaction for Engine Configurations Mounted above the Wing, Part 1. Interference Between Wing and Intake/Jet. AGARD CP-150, 1975.

6. Putnam, Lawrence E.: An Analytical Study of the Effects of Jets Located More Than One Jet Diameter Above a Wing at Subsonic Speeds, NASA TN D-7754, 1974.

7. Squire, H.B.; and Trouncer, J.: Round Jets in a General Stream. R.&.M. 1974, Brit. A.R.C., 1944.

8. Koning, C.: Influence of the Propeller on Other Parts of the Airplane Structure. Vol. IV, "Aerodynamic Theory," Ed. by W.F. Durand, Dover Publication.

9. Smith, Charles C. Jr.; Phelps, Arthur E. III; and Copeland, W. Latham: Wind Tunnel Investigation of a Large-Scale Semispan Model with an Unswept Wing and an Upper-Surface Blown Jet Flap. NASA TN D-7526, 1974.

10. Ishimitsu, Kichio K.: Investigation of Upper Surface Blowing Applied to High Speed Aircraft. AFFDL-TR-74-89, 1974.

11. Falk, H.: The Influence of the Jet of a Propulsion Unit on Nearby Wings. NACA TM 1104, 1946.

12. Putnam, Lawrence E.: Exploratory Investigation at Mach Numbers from 0.40 to 0.95 of the Effects of Jets Blown Over a Wing. NASA TN D-7367, 1973.

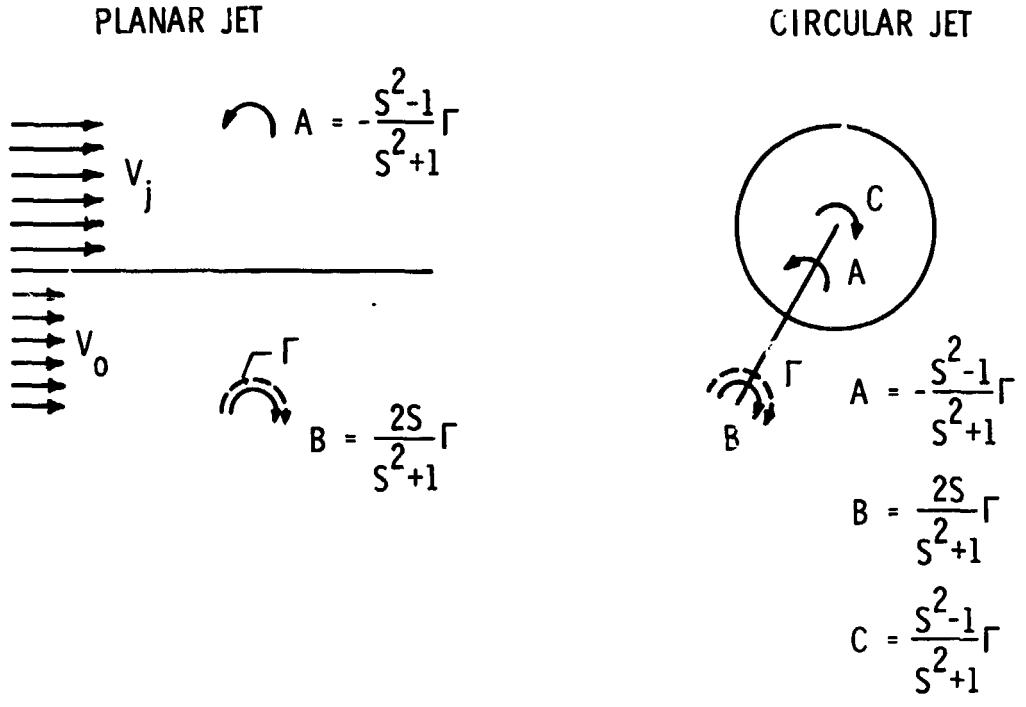

Figure 1.- Illustration of two-dimensional, inviscid jet interaction process.

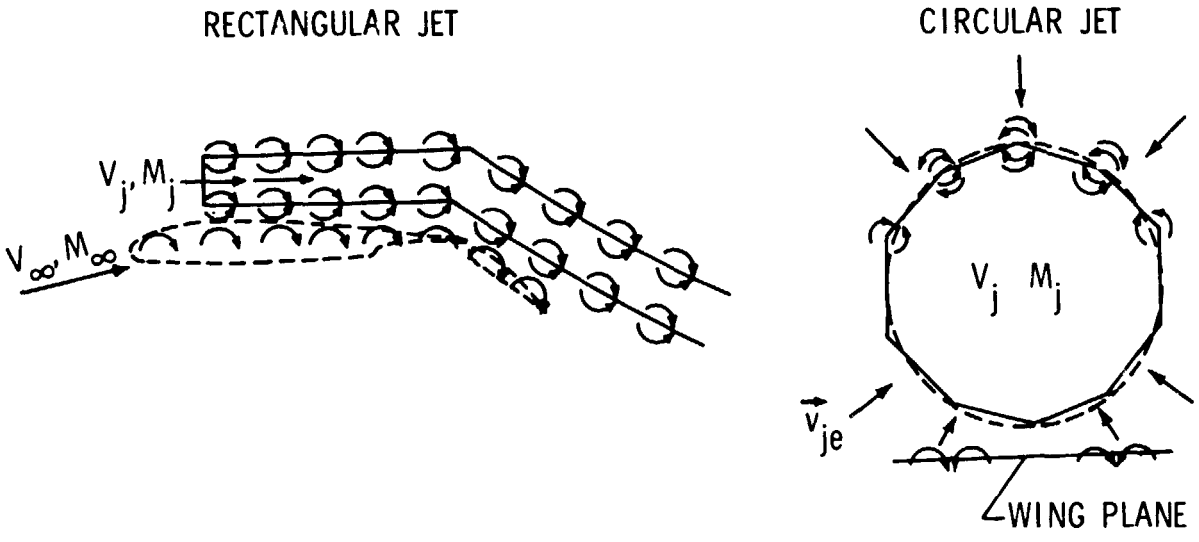

Figure 2.- Three-dimensional vortex model for jet interaction process.

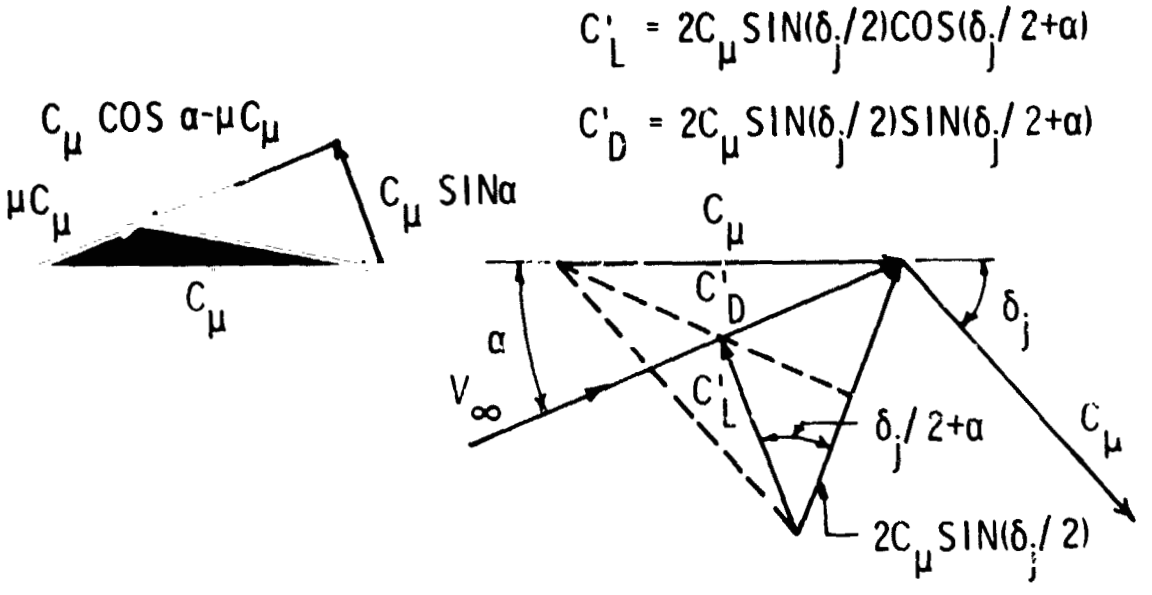

Figure 3.- Force components due to the Coanda jet reaction on USB configurations.

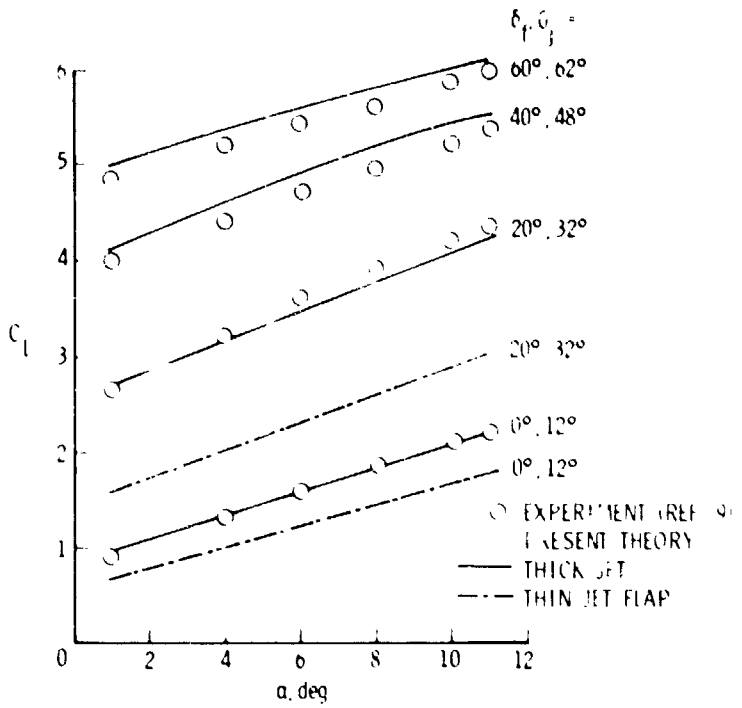

(a) Lift data.

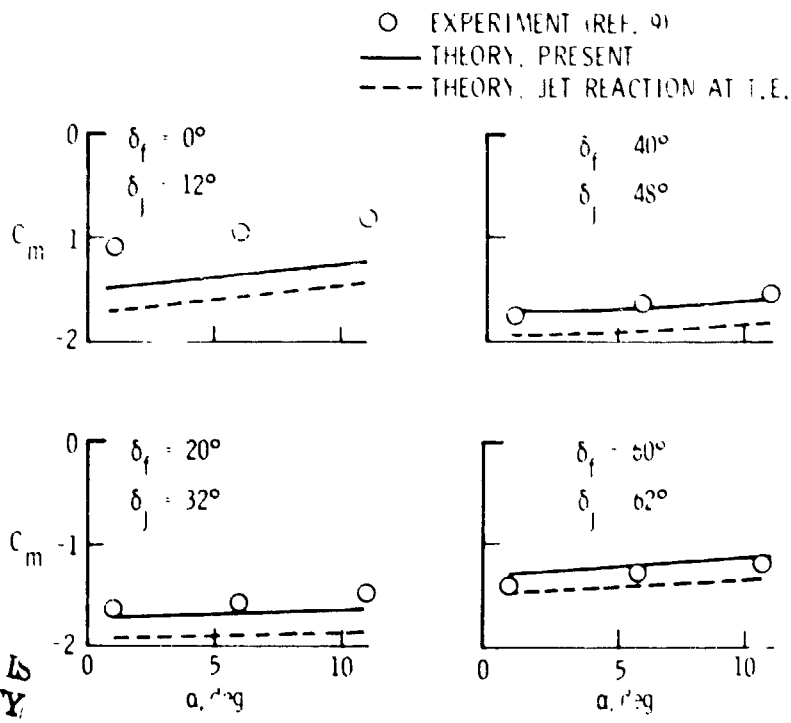

(b) Pitching moment data.

Figure 4.- Estimation of aerodynamic characteristics of a USB configuration for $C_\mu = 2$ (results obtained by adding the predicted jet-induced values to the experimental jet-off values).

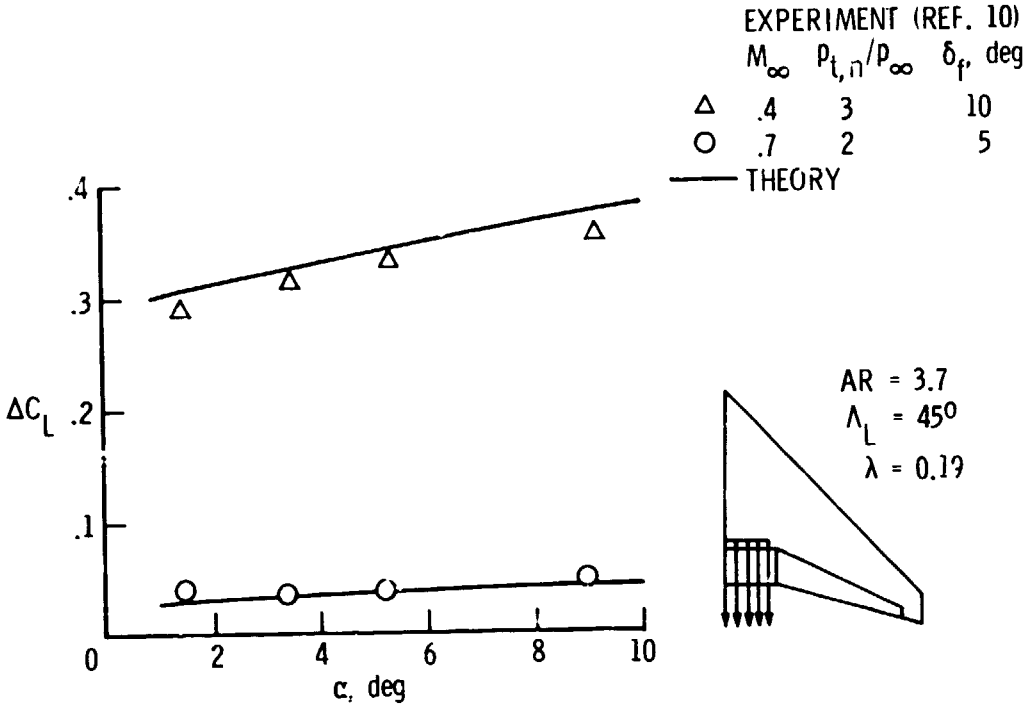

Figure 5.- Estimation of jet-induced lift for the vectored-thrust fighter configuration of reference 10.

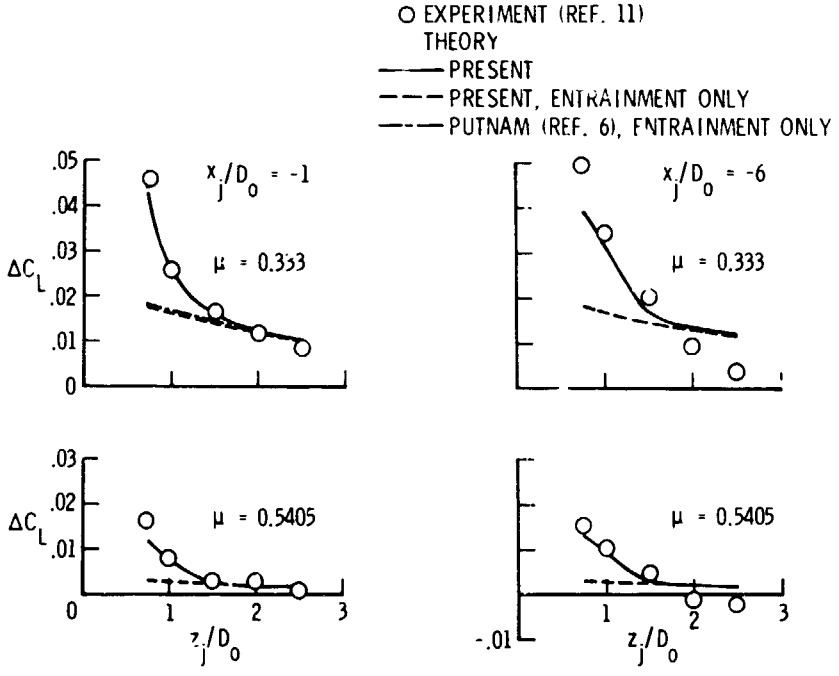

Figure 6.- Estimation of jet-induced lift for a rectangular wing having OWB. $\alpha = 0^o$; AR = 2.

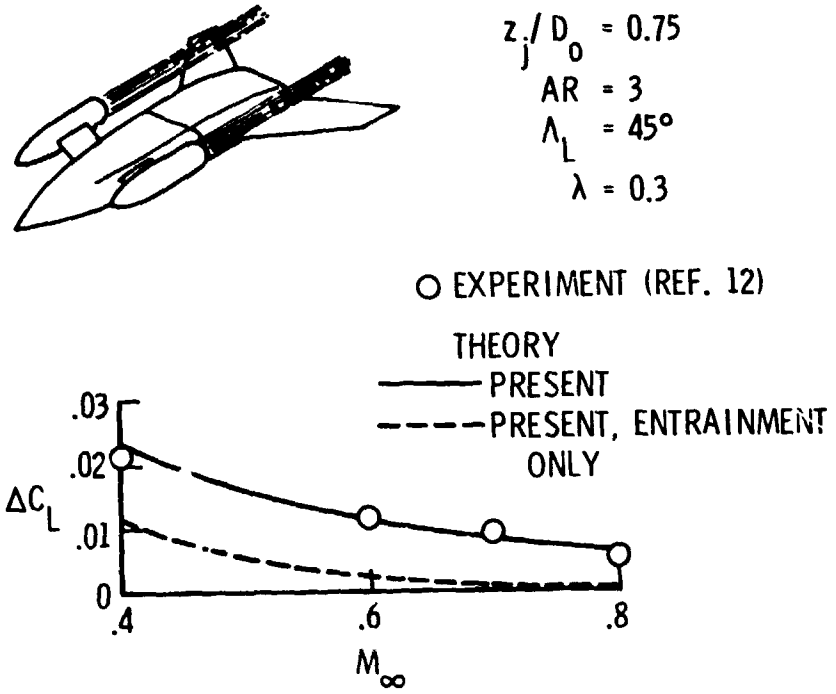

Figure 7.- Estimation of jet-induced lift for the OWB configuration of reference 12. $p_{t,n}/p_\infty = 1.9$; $\alpha = 0°$.

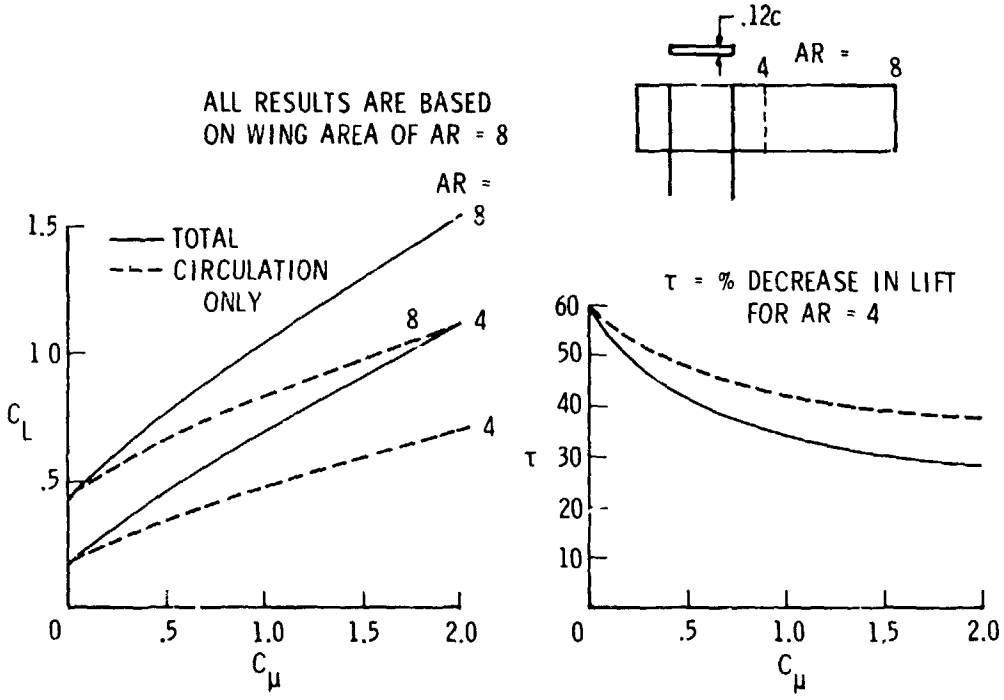

Figure 8.- Theoretical effect of aspect ratio on USB lift capability. $M_\infty = M_j = 0$; $\alpha = 2°$; $\delta_f = 0°$; $\delta_j = 10°$; NACA 65_1-412.

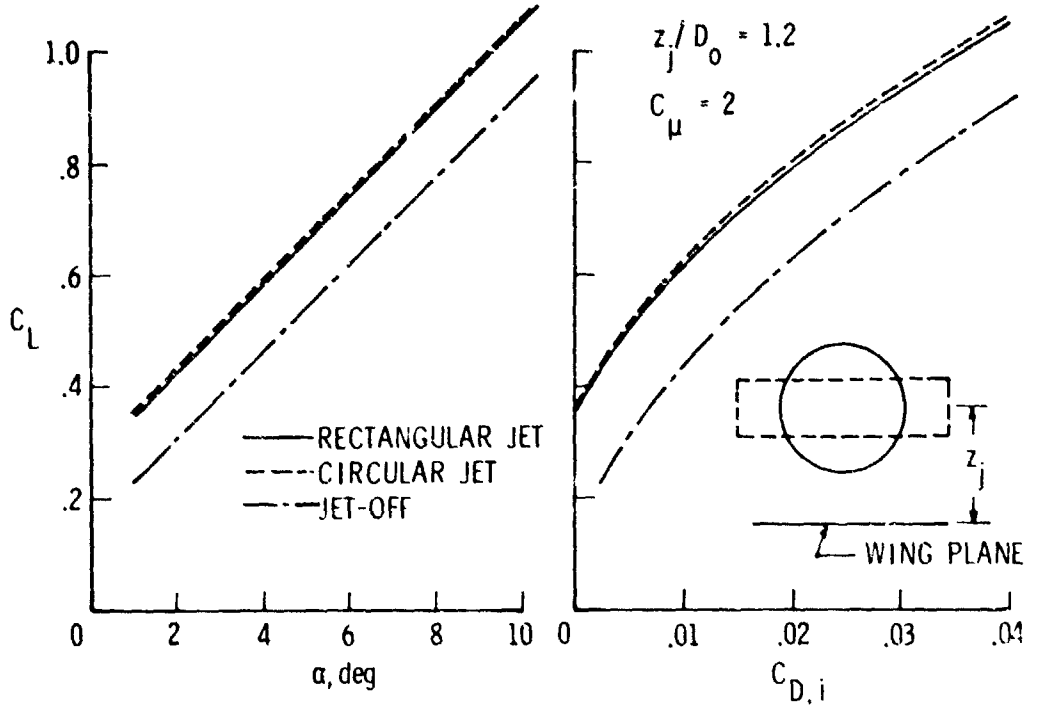

Figure 9.- Comparison of theoretical aerodynamics obtained by jets of rectangular and circular cross section on the configuration of reference 9. AR = 7.8; $\Lambda_L = 0^o$; $\lambda = 0.73$; $\delta_f = 0^o$.